Computational investigation on CO2 capturing capacity of N-doped and Na-decorated Graphdiyne

M. Asgari Bajgirani, Z. Biglari, Mehdi Sahihi

Computational Investigation on CO_2 Capturing Capacity of N-doped and Na-decorated Graphdiyne

M. Asgari Bajgirani[a], Z. Biglari[a,*], M. Sahihi[b,*]

[a] *Department of Physical Chemistry, Faculty of Chemistry, University of Lorestan, Lorestan, Iran*

[b] *Université Clermont Auvergne, CNRS, Clermont Auvergne INP, Institut de Chimie de Clermont-Ferrand, F-63000 Clermont-Ferrand, France*

***Corresponding authors**

Zeinab Biglari and Mehdi Sahihi

Email: biglari.z@lu.ac.ir and mehdi.sahihi@uca.fr

Tel.: +33 (0) 473407384

Abstract

Graphdiyne (GDY) is a newly discovered member of the two-dimensional carbon allotropes that has been proposed as a material for carbon dioxide (CO_2) capture and storage technology. The GDY structure is composed of several hybridized carbon atoms, and despite its superior electronic capabilities, modifying its structure can facilitate the advancement of its practical applications. This study considered, N-doping, Na-decoration, and their combinations as GDY modifications. The dispersion-corrected density functional theory (DFT-D2) approach was used to investigate the structural and electronic properties of the resultant adsorbents and their CO_2 adsorption behavior. Among three different N-doped structures, substituting an N atom for the Carbon with hybridization of SP^2-SP ($C_{SP^2\text{-}SP}$) produced the most stable N-doped GDY with E_{coh} = -7.23eV. Four different locations of GDY were decorated by Na atom, and the center of the H3 was identified as the most stable site with E_{ads} = -3.804eV. This site was also the most favorable for Na decorating of the N-doped GDY, with E_{ads} = -3.347eV. Moreover, the results indicated that when a single CO_2 was adsorbed on the Na-decorated GDY, the adsorption energy was -0.432eV, the highest value among the pristine and modified structures. However, evaluation of the maximum CO_2 capturing capacity of the systems revealed that N-doped GDY could capture eleven CO_2 molecules, ca. 68.92 Wt%, which makes it a potential candidate for future CO_2 capture, storage, detection, and removal applications.

Keywords: Graphdiyne (GDY), CO_2 capture, 2D carbon allotropes, Adsorption, DFT-D2.

1. Introduction

Modern industry is quickly evolving, and rising levels of CO_2 in the atmosphere necessitate the development of industrial systems for capturing and storing CO_2 along with other greenhouse gases (e.g., CO, CH_4, and NO_2) [1,2]. CO_2 capturing systems have utilized two-dimensional (2D) carbon-based materials such as graphene and graphyne [3–6]. Like the other members of the 2D carbon family, GDY has fascinating physicochemical features and is frequently employed in academic research [7–10]. The GDY's π-conjugated structure comprises of carbon hexagonal rings joined by diacetylene bridges (-C≡C-C≡C-), in which the sp–sp^2 hybridized carbon atoms serve as active sites. GDY has superior activity and selectivity compared to graphene, making it a suitable material for developing CO_2 capture techniques [11].

In 2010, Li et al. employed hexaethynylbenzene to synthesize GDY on a Cu foil surface via a cross-coupling process [12]. Due to its physicochemical qualities, there are various applications for GDY, including lithium-ion batteries, photocatalysis, electronic systems, energy storage, electrode materials, and hydrogen purification systems [8–10,13,14]. CO_2 capture capabilities of GDY are affected by many ways of tuning the structure, such as imposing defects, atom doping, and decorating [15,16]. The atom-doped GDY exhibits different charge transport, band gap, Fermi-level, and thermal stability than pristine GDY. In the literature, atoms such as B, P, N, and S have been utilized to prepare various kinds of doped GDY [10,17–19]. Wu et al. studied the performance of pristine and N-/B-doped GDY for detecting hazardous and greenhouse gases. They found that B-doped GDY had more sensitivity and selectivity for NO, NO_2, and NH_3 than pristine and N-doped GDY [16].

The decorating of metal atoms is another exciting method for improving the gas adsorption ability of GDY. Decorating atoms such as alkali, alkaline earth metals, and transition metals

can affect electron mobility by converting GDY from a narrow band-gap semiconductor to a semi-metallic state [20]. Using density functional theory (DFT) calculations, Feng et al. anchored Cu on B- and N-doped GDY to study the influence of decoration on electronic structures and CO_2-reduction reaction catalytic performance. Comparing the adsorption energies and charge transfer, they found that the Cu@N-doped GDY monolayer performs better for CO_2 reduction than the Cu@B-doped GDY monolayer [21].

Zou et al. investigated the effect of anchoring various transition metal atoms on the stability, electronic, and magnetic characteristics of N-doped GDY. They observed that electron mobility was increased, the metal atom binding strength was improved, and the stability of metal-decorated GDY was boosted. They also reported that Fe@2N-GDY provides the best catalytic performance with the lowest CO oxidization energy barrier [5]. Ebadi et al. studied the influence of Ca-decoration on the electronic and structural characteristics of GDY, and the adsorption behavior of H_2 molecules on pristine and Ca-decorated GDY, using DFT calculations. They concluded that calcium-decorated GDY is viable for hydrogen storage applications [20]. They also explored the adsorption behavior of methanol and CO molecules on intact GDY and Ca-GDY using DFT-D2 simulations. Their findings indicated that Ca-GDY might be a viable candidate for practical applications such as methanol and CO molecule capturing and storage [15]. Metal atoms have also been decorated on other 2D adsorbents to improv their adsorption of CO_2. Using DFT-D3 simulations, Darvishnejad et al. studied the effect of Sr, Sc, and Cr decoration on graphyne's structural and electronic characteristics of enhance CO_2 capture capacity. They investigated the adsorption energies of systems by placing the metal atoms at various locations of the graphyne frame. For CO_2 adsorption on the structures, the most stable modified structures were utilized as the adsorbent [4,22].

Yang et al. crafted a hetero junction composed of Bi_2WO_6 and GDY nanosheets and investigated the photo reduction CO_2 activity under simulated sunlight irradiation [23]. Their

findings indicated that the overall CO_2 conversion over the 2D/2D GDY/Bi_2WO_6 is 4.9 times higher than Bi_2WO_6. This was attributed to higher light adsorption, conductivity, and a wide interfacial contact area of the GDY, ensuring the improvement in photo-induced charge separation rates. They also claimed that the CO_2 adsorption of the hybrid structure was enhanced due to the increased specific surface area and micropores [23]. Dang et al. presented a computational method for generating a set of GDY-based frameworks, GDY-Rs and Li@GDY-Rs [24]. In the building blocks of GDY, they incorporated several functional groups (R: NH_2, OH, COOH, and F) and the doping metal atom (Li). Finally, a screening was carried out to identify the top candidates for CO_2 capture and sequestration applications. The combined DFT and grand canonical Monte Carlo (GCMC) simulations were used to examine the pore structure and morphology and the CO_2 adsorption and separation properties of these frameworks. They reported that the combination of Li-doping and hydroxyl group grafting results in an unanticipated synergistic effect for effective CO_2 capturing, with a CO_2 uptake of 4.83 mmol/g (at 298 K and 1 bar). They recommended Li@GDY-OH as one of the most promising materials for CO_2 capture and separation, with a selectivity of 13 for CO_2 over CH_4 (at 298 K and 1 bar) [24]. GDY's particular high π hybrid structure gives it uniform nanohole distribution, nonuniform electron distribution, excellent electrical conductivity and electron mobility, tunable band gaps, and high chemical stability. These attractive properties make graphdiyne a promising candidate for producing high-performance products and, as a combination for CO_2-capturing, a good candidate for photocatalytic solar fuel production and etcetera [25].

As mentioned above, the N-doped GDY exhibits different charge transport, band gap, Fermi-level, and thermal stability than pristine GDY [10,17–19]. Also, decorating the alkali metal atoms can improve the gas adsorption ability of GDY [20]. Hence, combining these two modifications may improve the CO_2 capturing property of GDY. To the best of our knowledge,

there is no detailed investigation about CO_2 capturing properties of N-doped and alkali metal-decorated GDY. Therefore, in the present study, three sorts of alterations were made to the GDY structure to propose a candidate for CO_2 capture and storage (CCS) technology, and exciting results were observed. We explored various GDY atoms and sites to discover the optimal position for doping the N atom and decorating the Na atom. The optimal configuration of the modified structures, which included N-doped, Na-decorated, and Na-decorated N-doped GDY, was then determined using the cohesive energy and metal atom adsorption energy. The structural and electronic properties of the best structures and their behavior in the adsorption of single and multiple CO_2 molecules were investigated. Finally, each structure's maximum CO_2 adsorption capacity was estimated to determine the structure with the best performance. Since most of the previously published research on CO_2 adsorption on GDY has focused on GDY decorated with transition metals, we hope that the novelty of the present study (using the alkali metals decorated GDY) could shed light in the CO_2 capturing and storage technologies.

2. Computational methods

The structural and electronic characteristics of pure and modified GDY structures, as well as their CO_2 adsorption properties, are examined in this study. First, several Na-decorated and N-doped GDY initial configurations were created and relaxed to determine the most stable geometry. The spin-polarized DFT approach was used for all calculations, including geometry optimization, Na adsorption, electronic properties, CO_2 capture, and charge distribution. The generalized gradient approximation (GGA) level of theory with the Perdew-Burke-Ernzerhof (PBE) [26] was used as the exchange-correlation functional. The double numerical plus polarization (DNP) basis set [27] was employed in the calculation using the DMol3 module [28], which is comparable with the 6-31G(d,p) basis set regarding computational accuracy [29]. The DFT-D2 approach, which was developed by Grimme, was utilized to account for dispersive inter-molecular interactions and long-range Van der Walls forces [30–32]. A 2×2×1

supercell of GDY unit cell with a vacuum space of 20 Å in the z-direction was built to avoid the interactions between layers. Integrations in the Brillouin zone were carried out using a 7×7×1 gamma-centered Monkhorst-Pack mesh of k-grid sampling. No symmetry limitations were imposed in geometry optimization, and all atoms were relaxed. The convergence tolerance for energy accuracy, maximum force, displacement, and global orbital cut-off radius was selected as 10^{-5} Ha, 2×10^{-3} Ha/Å, 5×10^{-3} Å, and 5.1 Å, respectively. Different parameters and diagrams like band structure, the density of State (DOS), partial DOS (PDOS), total DOS (TDOS), charge density, and Hirshfeld atomic charges were also presented for qualitative and quantitative interpretations of results.

The stability of N-doped GDY structures was determined by cohesive energy (E_{coh}) that can be calculated by Eq. 1 [29]:

$$E_{coh} = \frac{E_{N-dopedGDY} - n_C E_C - n_N E_N}{n_C + n_N} \quad (1)$$

where $E_{N\text{-}doped\ GDY}$, E_C, and E_N are the total energy of N-doped GDY, isolated carbon, and Nitrogen atoms, n_C and n_N are the numbers of carbon and nitrogen atoms, respectively. The adsorption energy (E_{ads}) of the Na atom adsorbed on the GDY sheet is calculated using Eq. 2 [4]:

$$E_{ads}^{Na} = E_{Na-decorated(N-doped)GDY} - E_{pristine(N-doped)GDY} - E_{Na} \quad (2)$$

where $E_{Na\text{-}decorated\ (N\text{-}doped)GDY}$, $E_{pristine(N\text{-}doped)GDY}$, and E_{Na} are the total energy of Na-decorated (N-doped) GDY, pristine (N-doped) GDY, and isolated Na atom, respectively. The average adsorption energy (E_{ads}) and the adsorption energy (E_s) per CO_2 molecule of each step are given by Eq. 3 and Eq. 4, respectively:

$$E_{ads} = \frac{1}{n}\left(E_{GDY-Na/N-nCO_2} - E_{GDY-Na/N} - nE_{CO_2}\right) \quad (3)$$

$$E_S = E_{GDY-Na/N-nCO_2} - E_{GDY-Na/N-(n-1)CO_2} - E_{CO_2} \quad (4)$$

where $E_{GDY\text{-}Na/N\text{-}nCO2}$, $E_{GDY\text{-}Na/N\text{-}(n\text{-}1)CO2}$, $E_{GDY\text{-}Na/N}$, and E_{CO2} are the total energy of the system containing the modified GDY and nCO_2, the system containing modified GDY and $(n\text{-}1)CO_2$, the modified GDY, and isolated CO_2 molecule, respectively and n is the number of the adsorbed CO_2 molecules. E_s shows the adsorption energy of the n^{th} CO_2 onto the structure of $(n\text{-}1)^{th}$ step. Upon the value of E_s becoming smaller than 0.1eV, the adsorbent no longer has the sufficient ability to adsorb the subsequent CO_2 molecule [4]. Then, the addition of CO_2 molecules to the adsorbent is stopped.

CO_2 capture capacity was calculated using the following equation:

$$CO_2 \text{ capture capacity}\left(wt.\%\right) = \left[\frac{M_{co_2}}{M_{co_2} + M_{host}}\right] \times 100 \quad (5)$$

where Mco_2 and M_{host} are the total mass of the adsorbed CO_2 molecules and the mass of the adsorbent.

As shown in **Fig. 1**, the symmetric structure of GDY composes of an sp^2-hybridized hexagonal carbon ring and six sp-hybridized acetylenic carbon chains [20]. There are three types of carbon atoms in the structure: C1(C_{SP^2}-$_{SP^2}$), C2(C_{SP^2}-$_{SP}$), and C3(C_{SP}-$_{SP}$) due to their different types of hybridization. The position of each of these structural carbons and the length of the bonds connecting them were illustrated in **Fig. 1**. To improve the CO_2 adsorption capability of the structure, the GDY structure was modified, and the electronic and structural effects of the modifications were investigated. On pure GDY, Discrete structural modifications such as N-doping and Na-decoration were done in different places on the GDY sheet.

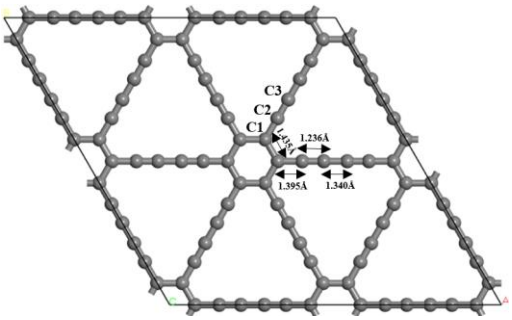

Fig. 1. The optimized structures of pristine GDY with various C-C bond lengths.

3. Result and discussion

3.1. Evaluation of the structural and electronic properties of pristine and modified GDY

In the 2×2×1 supercell structure of GDY, there are 72 carbon atoms. Unlike graphene, as a conductor, GDY has a non-zero band gap at the gamma point (Γ) [33] and is hence a semiconductor. Structural symmetry of GDY can lead to electronic symmetry; applying impurities in the structure, such as atom decorating or doping, might induce a deviation from this symmetry, improving the gas adsorption capabilities of the adsorbent. Three structural alterations were applied to the GDY structure by doping the N atom, decorating the Na atom, and combining these two modifications. The places where these alterations are made are shown in **Fig. 2**. In the GDY structure; three atomic sites are the candidates for replacement with nitrogen atoms (**Fig. 2**). Furthermore, for placing the decorative Na atom, the sites H1, H2, H3, and B were chosen. **Table 1** shows the energy released by each modified structure after geometry optimization.

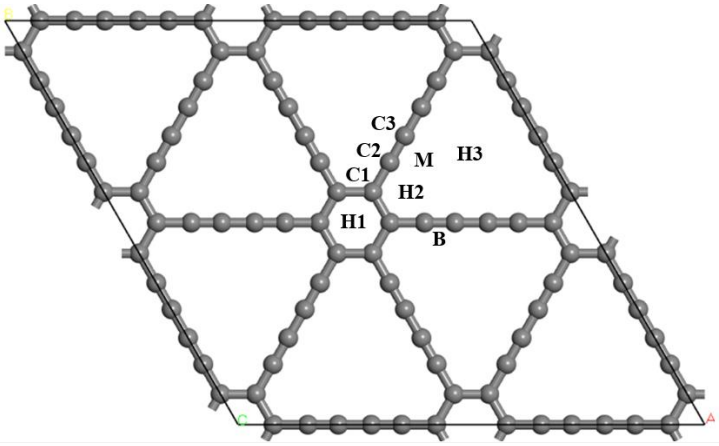

Fig. 2. Three types of carbon atoms (C1, C2, and C3) and the five possible sites are labeled by H1, H2, H3, B, and M.

Table 1. Binding and adsorption energies of modified structures (N doped-, Na decorated-, and Na decorated-N doped GDY) at different binding and adsorption sites.

Structure	Cohesive Energy (eV)			Adsorption energy(eV)						
	C1	C2	C3	H1		H2		H3		B
				d(Å)=0	d(Å)=1.5	d(Å)=0	d(Å)=1.5	d(Å)=0	d(Å)=1.5	d(Å)=1.5
N-doped	-7.216	-7.231	-7.226	--	--	--	--	--	--	--
Na-decorated	--	--	--	-2.986	-2.963	-3.805	-3.802	-3.804	-3.797	-3.502
Na-decorated	--	-7.231	--	-2.759	-2.759	-3.346	-3.344	-3.347	-3.344	-3.334

The pristine and most stable modified structures (N-doped GDY, Na-decorated GDY, and Na-decorated-N-doped GDY) are called S1, S2, S3, and S4, respectively, in the following sections. As can be seen, doping the N atom with cohesive energy (E_{coh}) of -7.231eV instead of the C2 carbon atom resulted in the most stable structure among the modified systems. Additionally, with adsorption energy (E_{ads}) of -3.804eV, decorating the Na atom in the H3 site is the most stable decorated structure. Finally, the Na atom was decorated on several sites of the best S2 structure, and as shown, the H3 site is the best site among the double-modified structures, with

an adsorption energy of -3.347eV. The bond length and structure energy, cohesive energy, gap energy (E_g), and Fermi level (E_f) are reported for the most stable structures in **Table 2**. Also, **Fig. 3** represents the optimized geometrical forms.

Table 2. Structural and electronic properties of pristine GDY and best conformations of the modified GDYs.

Structure	C1-C1(Å)	C1-C2(N)(Å)	C2(N)-C3(Å)	C3-C3(Å)	E_{coh}(eV)	E_{ads}(eV)	E_g(eV)	E_f(eV)
S1	1.236	1.395	1.435	1.340	-7.709	--	0.445	-5.223
S2	1.197	1.347	1.438	1.323	-7.231	--	0.000	-4.906
S3	1.239	1.394	1.435	1.339	--	-3.804	0.000	-4.850
S4	1.209	1.339	1.439	1.315	--	-3.347	0.000	-4.841

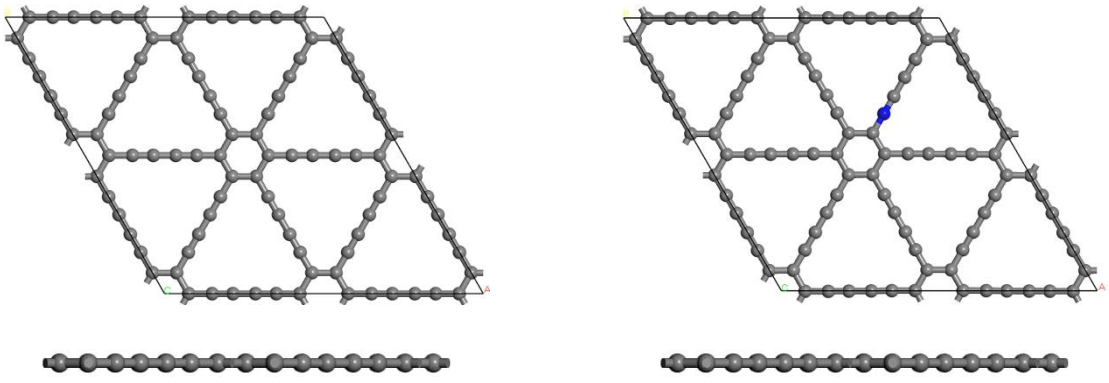

(a)

(b)

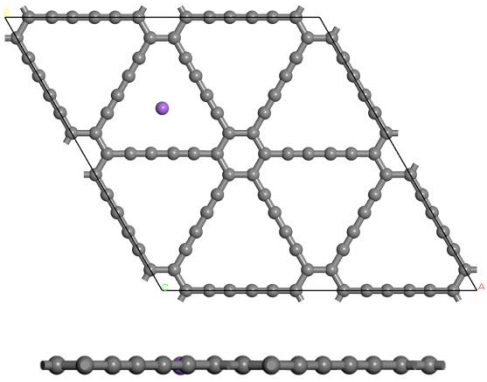

(c)

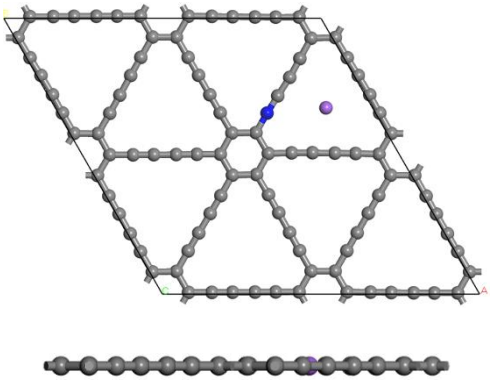

(d)

Fig. 3. The optimized geometrical structure of **(a)** pristine GDY and modified GDY **(b)** S2, **(c)** S3, and **(d)** S4. The gray, blue and purple balls represent C, N, and Na atoms, respectively.

The bond length of nitrogen to the neighboring atoms is directly affected by the smaller radius of the N atom and the difference in electronegativity between C and N atoms. **Table 2** shows that in the S2 structure, the length of the C1-C1, C1-N, and C3-C3 bonds reduces while the length of the N-C3 bond increases. The existence of N-C bonds instead of C-C bonds in the S2 structure and the resulting change in electron distribution can be linked to the decrease in cohesive energy. An increase in the length of the N-C3 bond can be attributed to the partial occupation of antibonding orbitals. However, because nitrogen is more electronegative than carbon, a decrease in the covalent nature of the bond leads to electrostatically stronger N-C bonds [34,35]. The decorating of Na on the structures S1 and S2 has a minor impact on the geometrical structure of GDY; this is due to a shift in the charge distribution caused by the charge donation of the 3s electrons of the Na atom to the π/π^* states. Decorating Na on structure S1 also has higher adsorption energy than decorating Na on structure S2. Graphdiyne, like graphyne, has sp-hybridized carbons, unlike graphene, which has sp^2-hybridized carbons. For this reason, there are π/π^* states in the p_x-p_y direction in-plane and p_z orbitals out-of-plane. As a result, it has π/π^* states that can be very effective for creating stronger interactions with metal and other adsorbing [36,37].

The frequency calculations were performed for S2 and S3 structures at different sites (H1, H2, H3 and B) and at intervals of 0 and 1.5 Å for Na-decorated and N-doped (C1, C2, and C3) configurations. The results confirm that the best locations for N-doping and Na-decoration are C2 and H3 sites, respectively (**Table 3**).

Table 3. The lowest calculated vibrational frequencies (cm^{-1}) related to and N-doped (C1, C2, and C3) and Na-decorated in 4 sites (H1, H2, H3 and B).

Vibrational frequencies (cm^{-1})										
Structure	C1	C2	C3	H1		H2		H3		B
				d(Å)=0	d(Å)=1.5	d(Å)=0	d(Å)=1.5	d(Å)=0	d(Å)=1.5	d(Å)=1.5
S2	29.54	30.88	28.30	---	---	---	---	---	---	---
S3	---	---	---	23.62	21.41	27.19	27.07	31.43	30.18	30.57

As seen in **Table 1**, changes in electronic characteristics cause the band gap to have zero in all modified structures. Different band gap values for the GDY structure have been reported in theoretical research due to different computational settings, such as different exchange correlations. The spin-polarized direct band gap for the GDY monolayer obtained in this study is 0.445eV, which agrees with previous theoretical and experimental results [20,38]. Additionally, **Table 1** indicates that making these modifications increases the Fermi level and causes moving towards the conduction band, indicating that the modified structures are n-type semiconductors or have improved semi-metallic characteristics [20]. The Fermi level of the S4 structure shows the most change, confirming its higher conductivity compared to the other structures (S1 to S4), which shows that this structure has a higher conductivity than the rest. The change in these electronic properties can be justified by examining the electron band structure diagram for all four structures, as shown in **Fig. 4**. Pure GDY is a direct semiconductor (0.445eV) which is consistent with other previous studies [39], N-doping and Na-decorating affected the electron band structure, causing the conduction bands to cross the Fermi energy level entirely. Also, the Fermi line has been cut by the conduction bands. This also indicates that all modified structures have a semi-metallic electronic character with zero band gap. Moreover, the Fermi level is set to zero [29]. Indeed, the presence of nitrogen and alkali metal

atoms causes additional electrons, and a new bonding orbital is created. The energy of this new bonding orbital would be between the previous HOMO and LUMO orbitals. Therefore, the value of Egap is reduced to make GDY a conductive material.

The conductivity is exponentially proportional to the value of E_{gap}, and the conductivity increases with the decrease of E_{gap}. The E_{gap} value which is a good estimate of conductivity, could be calculated using the HOMO-LUMO difference. The electric conductance can be related to E_{gap} as follows [40]:

$$\sigma \propto e^{\frac{-Eg}{kT}} \tag{6}$$

where σ depicts the electrical conductance, k is Boltzmann's constant, and T represents the absolute temperature. Thus, at a given temperature, the electrical conductance is inversely proportional to the E_{gap}.

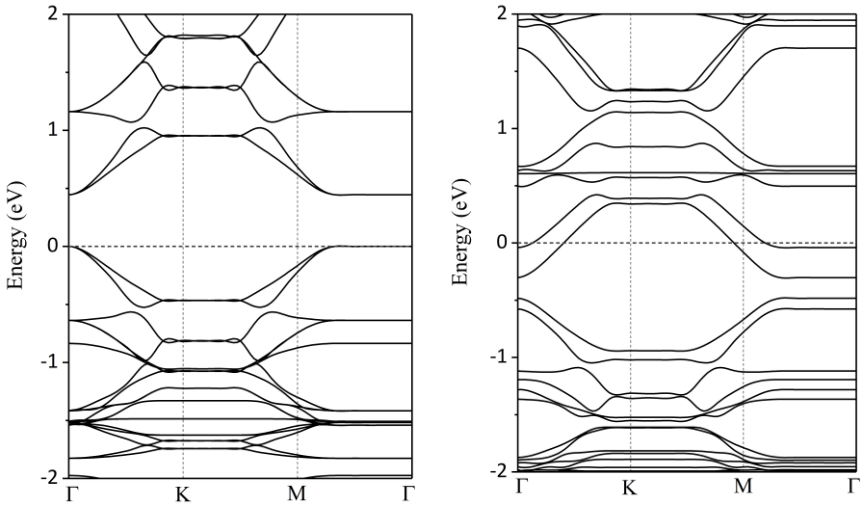

(a) **(b)**

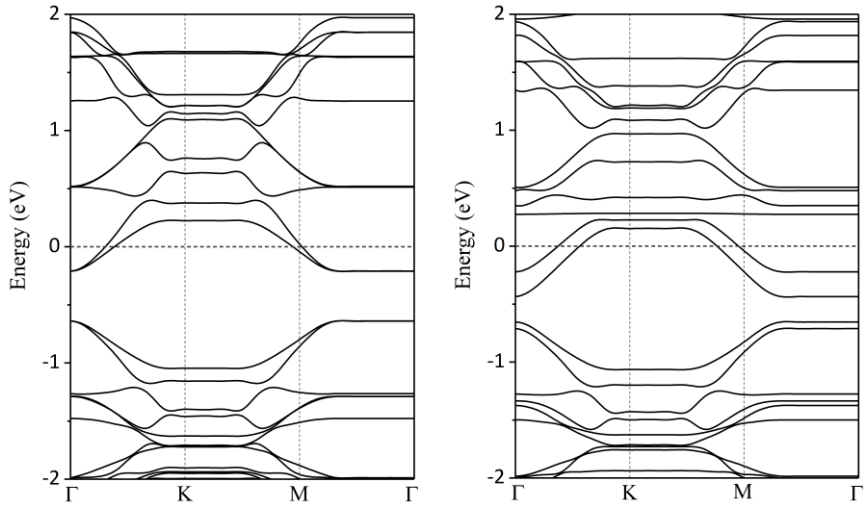

(c) **(d)**

Fig. 4. Band structure of diagrams: **(a)** S1, **(b)** S2, **(c)** S3, and **(d)** S4 structures. The Fermi level was set to zero.

The Hirshfeld charges of C1 and C3 atoms, the adjacent atoms of N, changed from $0.023e^-$ and $0.013e^-$ to $0.062e^-$ and $0.134e^-$, respectively, in the S2 structure, as shown in **Fig. 5**. It can be inferred that the electron distribution is inclined from the six carbon-ring to the bridge. This could be due to the N atom's withdrawing electrons from the carbon skeleton, increasing the negative charge of the N atom to $-0.004e^-$. The doping of N atoms disrupts the symmetry of the electric charge in the structure.

Because of the presence of the Na atom, the charge distribution in the entire structure has changed, with the positive (negative) charge of C1 (C2) atoms decreasing and the negative charge of the C3 atom increasing. After decoration, the charge distribution is transferred from the Na atom across the structure, giving this atom a charge of +0.482. However, the electric charge symmetry of the structure is preserved, and only the electric charge values of each atom have changed by a certain amount. Carbon atoms C1, C2, and C3 had their electric charge values modified from $0.023e^-$, $-0.010e^-$, and $-0.03e^-$ to $0.006e^-$, $-0.007e^-$, and $-0.042e^-$,

respectively. The quantity of positive charge Na in the S4 structure has changed slightly from the S3 structure due to the combined effect of doping N and decorating Na.

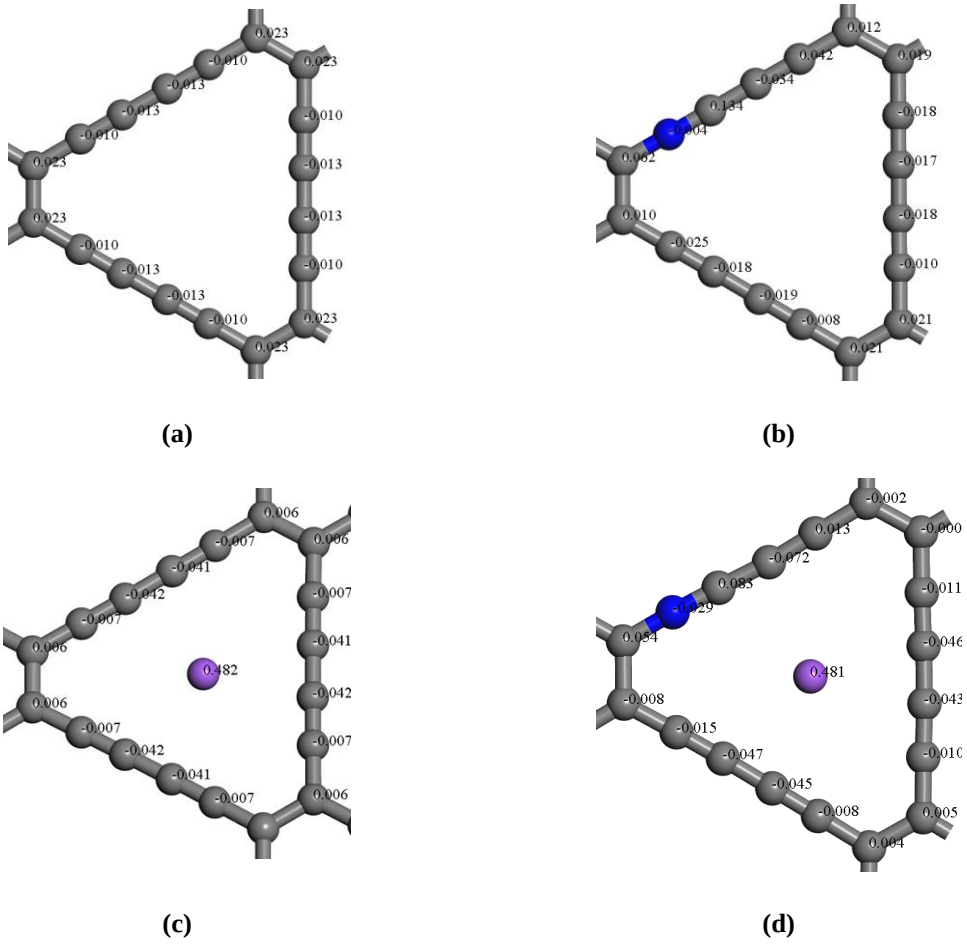

Fig. 5. Hirshfeld charges of C atoms and modifying atoms (N and Na) in **(a)** S1, **(b)** S2, **(c)** S3, and **(d)** S4 sites.

The TDOS diagram can reveal information about the bonding mechanism, interactions between the constituent atoms of the structure, contributions of C atoms with various hybridizations, and charge transfer interaction states. The TDOS and PDOS diagrams for each carbon atom and the modifying atoms (N, Na) are shown in **Fig. 6.** Fermi level was set to zero in all diagrams. The contribution of the s- and p-orbitals around the Fermi energy level increases due to the presence of the N atom with a higher number of electrons in the p-orbital, according to

the TDOS diagrams for S1 and S2. The charge density was also broadened at various energy levels. Doping N as an impurity in the structure has increased electron density at energy levels above the Fermi level. The electronic effect of the adsorption of Na onto the GDY structure was along with a low (high) change in the charge density of s-orbital (p-orbital), and charge distribution has also shifted towards higher energies. In the decorated structures, the charge distribution in the conduction band is increased compared to the S1 structure; this increase is higher for the S3 system.

The contribution of the p-orbital of the three carbon atoms increases near the Fermi level, as shown in the PDOS diagram of **Fig. 6**. The charge density distribution of the GDY in the s-orbital is in the energy range of -6 to -20eV, whereas the energy range of S2 is in the range of -6 to -22eV. The charge density in the p-orbital of the C1 atom decreases in N-doped structures (i.e., S2 and S4). The charge density in the s- and p-orbitals decreases, and the charge density is distributed over a broader energy range. Overall, the increase in the charge density in orbitals with energies higher than the Fermi level results in the higher electrical conductivity of the S3 structure. The PDOS diagram of the Na atom in both S3 and S4 structures shows that the charge density is lower in S4; this agrees with the electric charge of the atom, implying that Na has donated more electric charge to the atoms of the GDY structure.

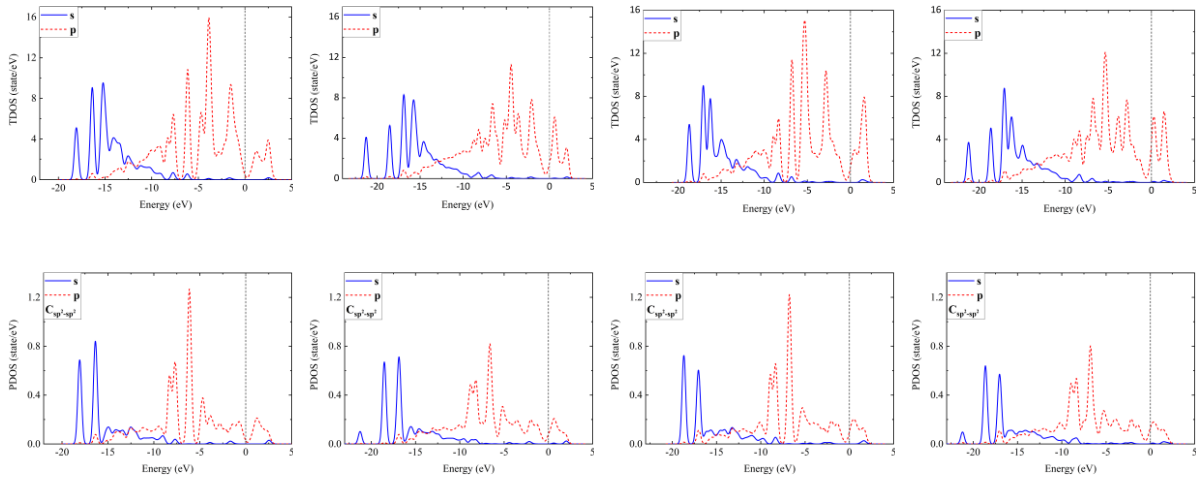

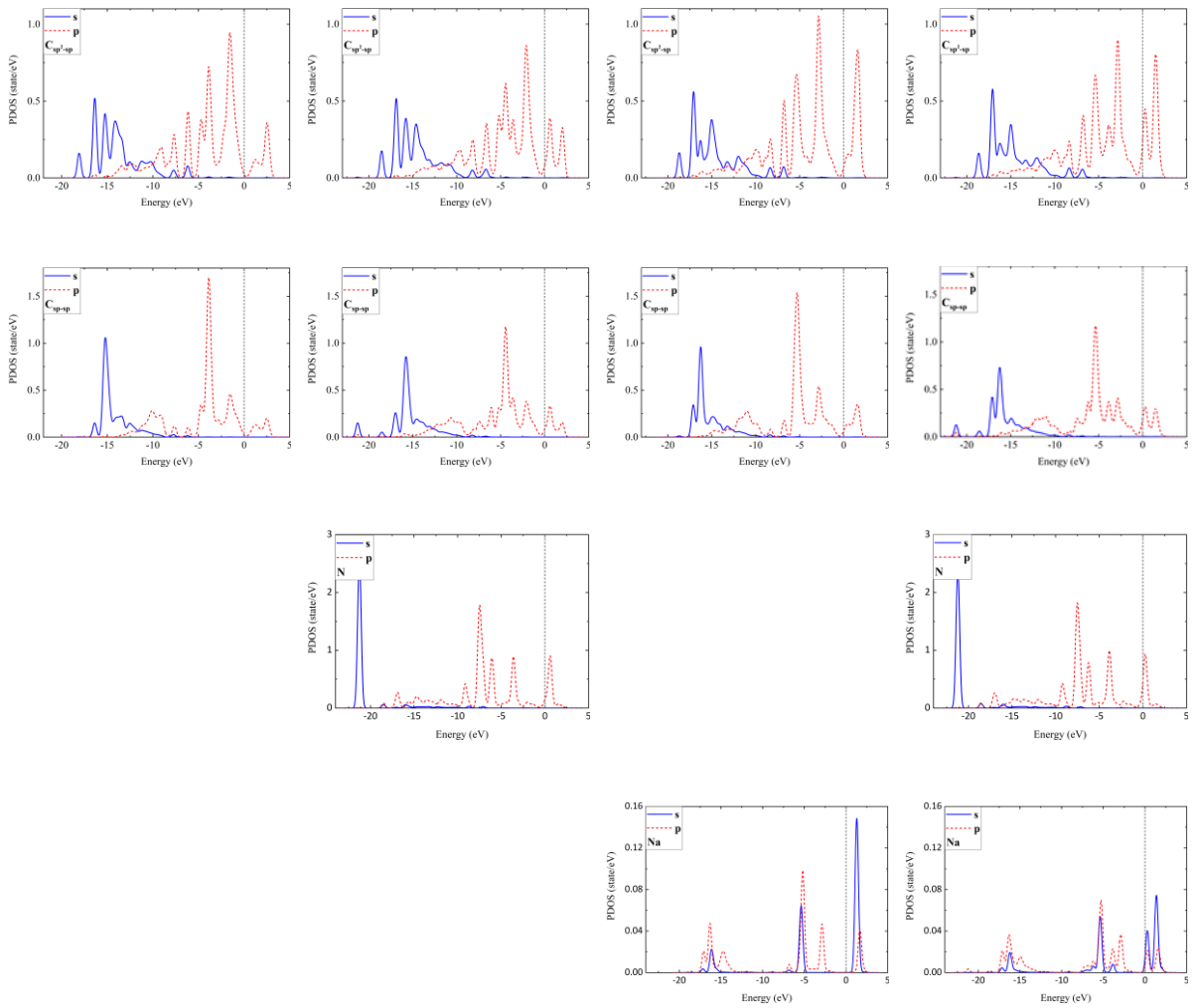

(a) **(b)** **(c)** **(d)**

Fig. 6. TDOS and PDOS diagrams: **(a)** S1, **(b)** S2, **(c)** S3, and **(d)** S4.

3.2. Adsorption of single CO_2 molecule onto the pristine and modified GDY

To find the best site for capturing the single CO_2 molecule on pristine and modified GDY structures, the CO_2 molecule was placed horizontally and vertically in different sites, as shown in **Fig. 2.** The obtained structures were optimized, and the resulting adsorption energies are presented in **Table 4.** The S4 structure provides better adsorption properties among the modified structures due to higher adsorption energy. CO_2 is a linear molecule with $D_{\infty}h$ symmetry. During the horizontal interaction with the active sites of the GDY surface, the

oxygen atoms could also be placed in front of the active sites. On the other hand, the CO_2 molecule was placed horizontally and vertically at various points described above, and the system was allowed to calculate the optimized structure by minimizing the energy.

Table 4. Adsorption energy of single adsorbed CO_2 on the pristine and modified GDY at different sites.

Structure	Adsorption energy(eV)									
	H1		H2		H3		B		M	
	V	H	V	H	V	H	V	H	V	H
S1	-0.178	-0.181	-0.191	-0.185	-0.270	-0.291	-0.172	-0.174	--	--
S2	-0.161	-0.158	-0.173	-0.268	-0.195	-0.271	-0.218	-0.221	--	--
S3	-0.163	-0.187	-0.285	-0.287	-0.415	-0.432	-0.14	-0.162	--	--
S4	-0.163	-0.178	-0.351	-0.347	-0.439	-0.357	-0.242	-0.233	-0.416	-0.442

Table 4 indicates that H3 is the best site for adsorbing CO_2 onto structures S1, S2, and S3, while M is the best adsorption site for S4 (the site between H3 and the position of the C2 atom). For all the systems (adsorbent + CO_2), **Table 5** shows the adsorption energy, the length of the C-O bonds, the distance of the CO_2 molecule from the adsorbent surface, and the angle O-C-O and the charge of each CO_2 atom. The calculated bond length and angle for free CO_2 molecule are 1.175Å and 179.66° respectively, which is in line with 1.16Å and 180° from experiments[41] and 1.177Å and 179.87° from previous theoretical calculations [42]. As can be observed, the C-O bond has a longer bond length when C is close to the adsorbent, and this bond length reaches a maximum value in the S4 structure. A single CO_2 molecule adsorbed in the closest site (farthest) to the S2 (S3) surface, showing that the CO_2 molecule was affected by the attraction (repulsion) force of the N (Na) atom. The effect of repulsion and attraction on CO_2 in the S4 structure has resulted in the point between the Na and N atoms being the optimal

site for CO_2 capture onto the structure. Furthermore, comparing the angle of the CO_2 molecules reveals that the CO_2 molecule has the biggest angle change in the S2 structure, and the charge of the O atom has the highest negative value. When adsorbed on the S3 structure, the carbon atom in the CO_2 molecule is most positively charged.

Table 5. The capture of single CO_2 on the S1, S2, S3, and S4 structures; Adsorption energy (E_{ads}), C-O bond length (L_{C-O}), the distance between CO_2 and GDY (d), O-C-O angle, and Hirshfeld charge of N, Na and O in CO_2 molecule (n: near, f: far from GDY).

structure	E_{ads}(eV)	L_{C-O} (Å)		d(Å)	A_{O-C-O}	Hirshfeld charges (e)				
		n	f			O(n)	C	O(f)	N	Na
S1	-0.232	1.750	1.75	2.514	179.646°	-0.145	0.29	-0.152	--	--
S2	-0.301	1.176	1.17	2.250	179.173°	-0.159	0.28	-0.149	-0.005	--
S3	-0.432	1.179	1.16	3.189	179.283°	-0.119	0.32	-0.106	--	0.405
S4	-0.391	1.180	1.16	2.864	179.189°	-0.121	0.31	-0.103	-0.025	0.437

The final spatial orientation and adsorption site of the CO_2 molecule in the structures are shown in **Fig. 7**. The CO_2 molecule is horizontal in its most stable state on structure S1; however, it is tilted with respect to the adsorbent structure in the modified systems.

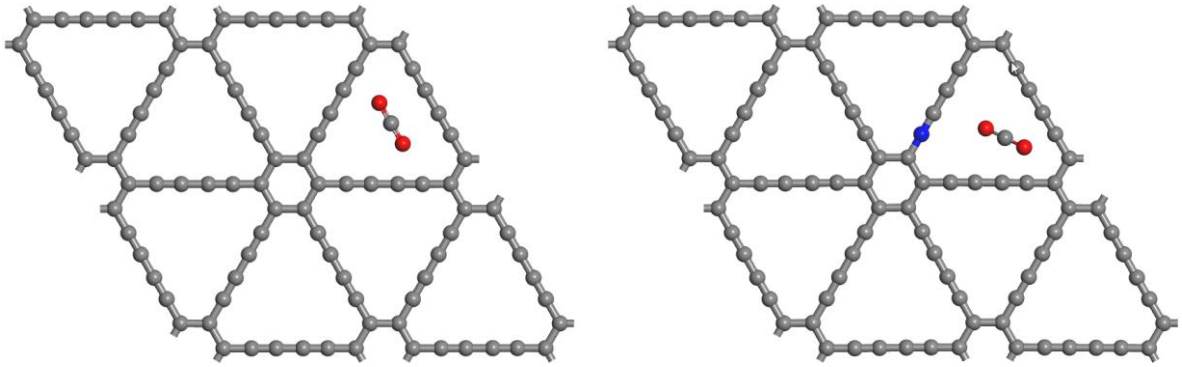

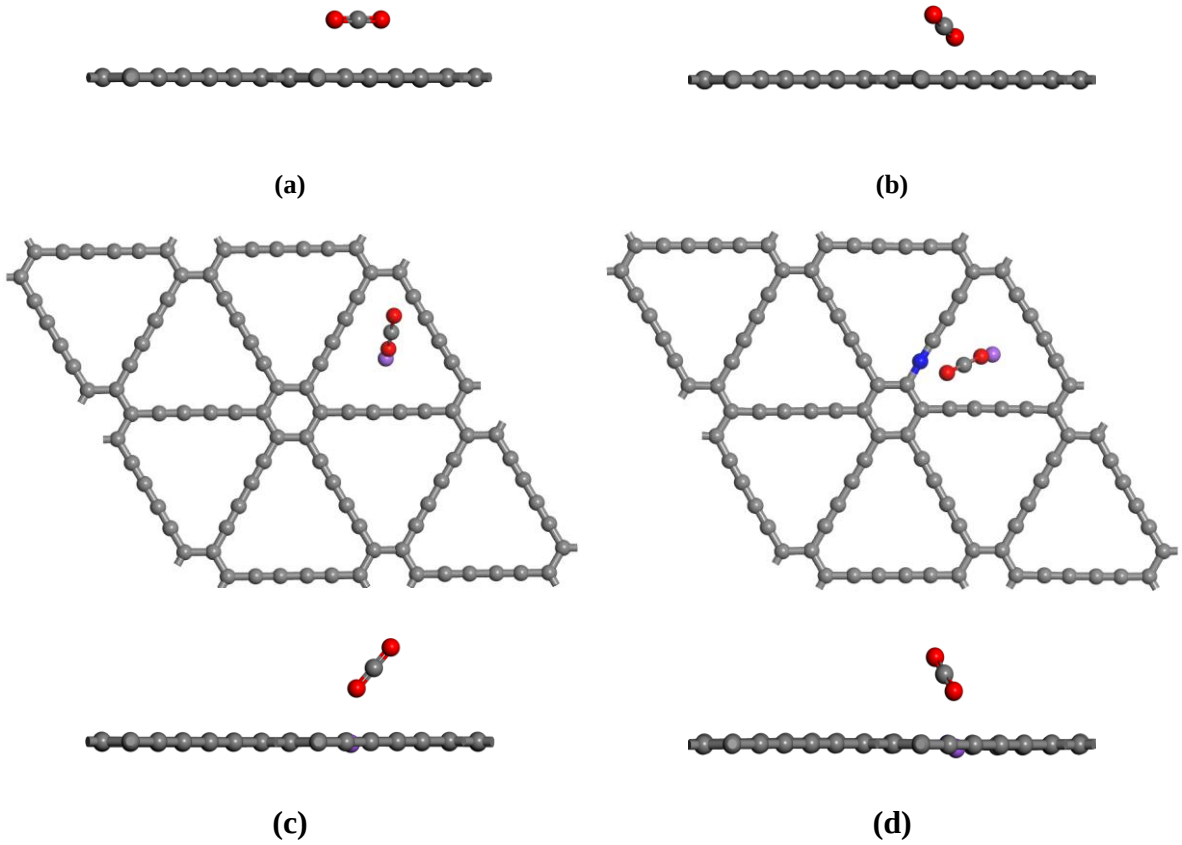

Fig. 7. Top and side views of the most stable site and orientation of the adsorbed CO_2 onto **(a)** S1, **(b)** S2, **(c)** S3, and **(d)** S4 structures.

The electric charge of each atom in the structure and molecule of CO_2 is shown in **Fig. 8**. The charge distribution of the carbon atoms near the gas molecule has changed slightly, as can be seen. Because of the difference in Columbic energy and, as a result, the value of adsorption energy released, the energy difference impacts structural stability. The nearer O atom to Na (N) in the S4 structure has a higher (lower) negative charge. When comparing S3 and S4 (S2 and S4), we can see that S4 has a more positive (negative) charge on the Na (N) atom.

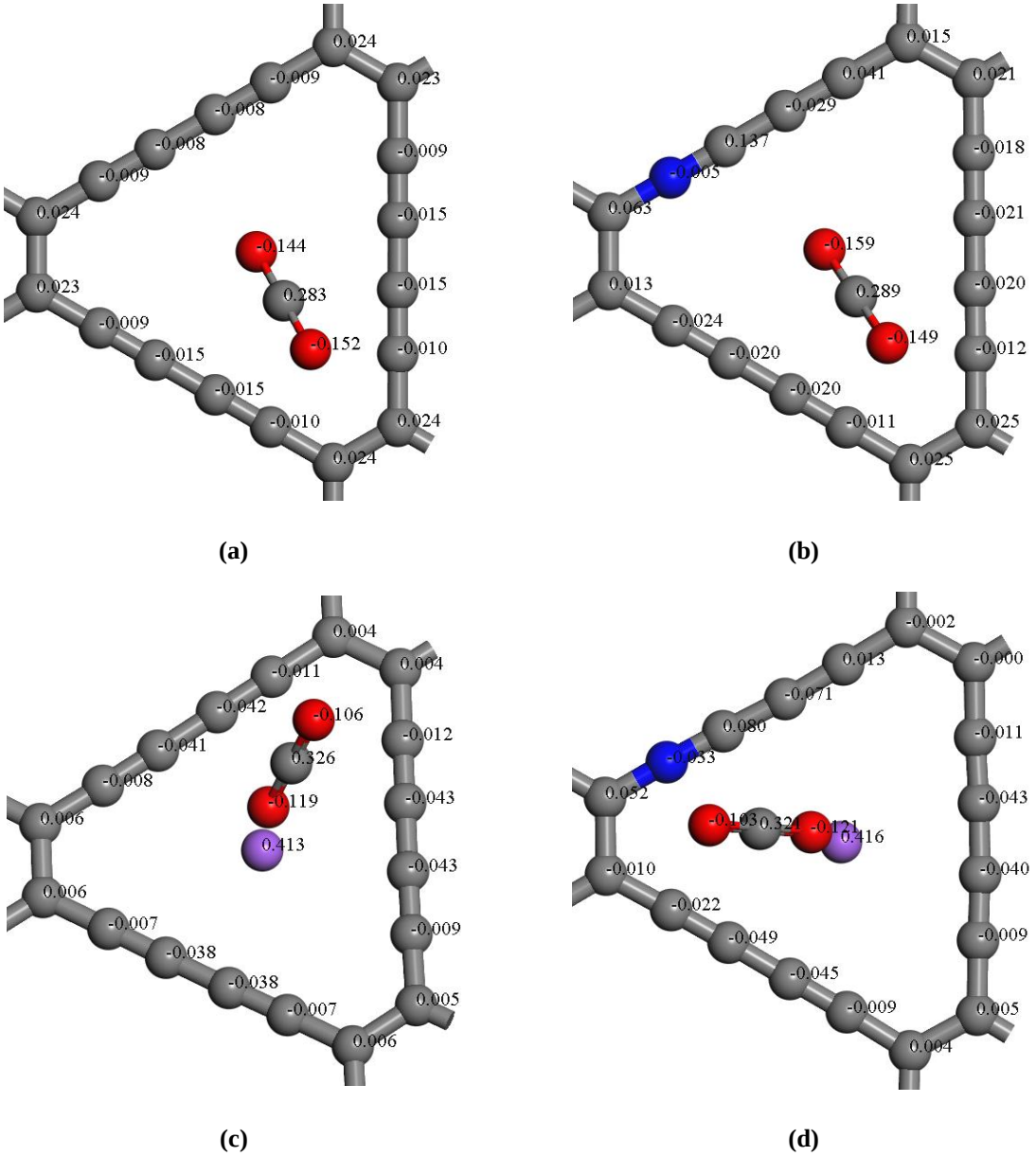

Fig. 8. Hirshfeld charges of C of structures, modifying atoms (N and Na) and the atoms of the CO_2 molecule in **(a)** S1 **(b)** S2, **(c)** S3, and **(d)** S4 structures.

To further understand the nature of the interaction between the CO_2 molecule and the structure, the PDOS diagrams of CO_2 adsorbed on the pristine and modified GDY structures are displayed in **Fig. 9**. The contribution of each type of structural carbon atom, as well as modifying atoms (N, Na), and CO_2 in the states, was taken into account in these images.

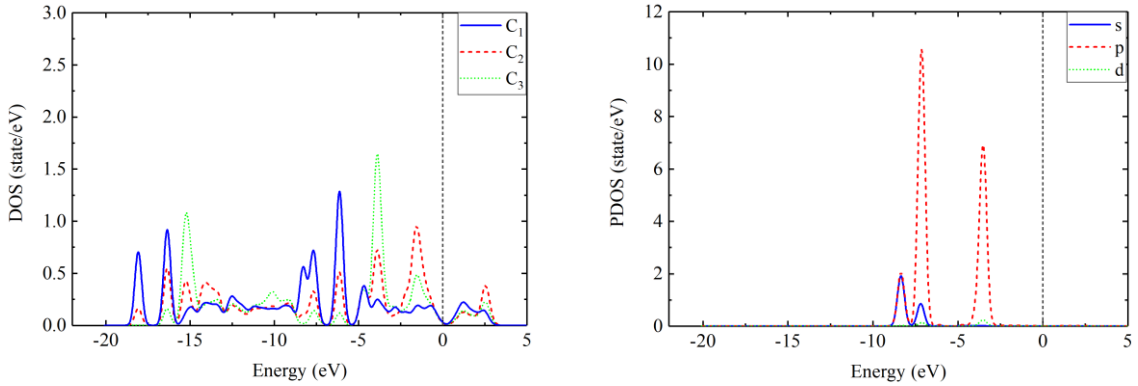
DOS (state/eV)
Energy (eV)
C1
C2
C3
PDOS (state/eV)
Energy (eV)
s
p
d

(a)

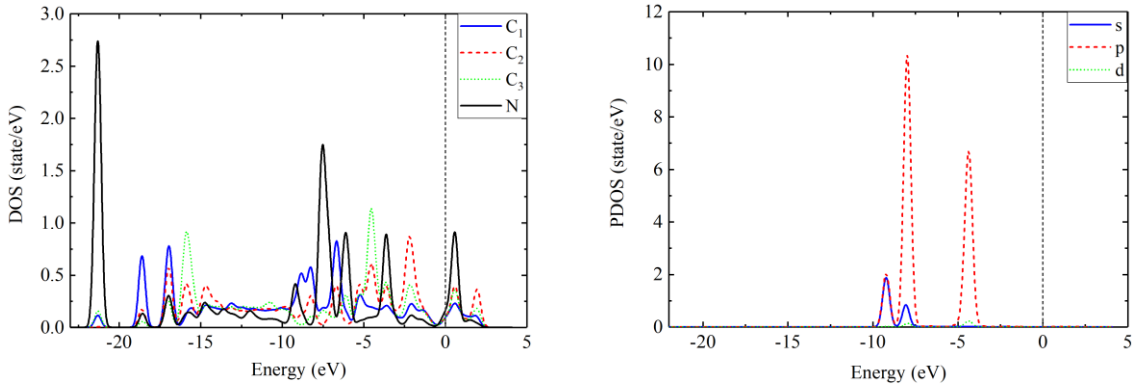
DOS (state/eV)
Energy (eV)
C1
C2
C3
N
PDOS (state/eV)
Energy (eV)
s
p
d

(b)

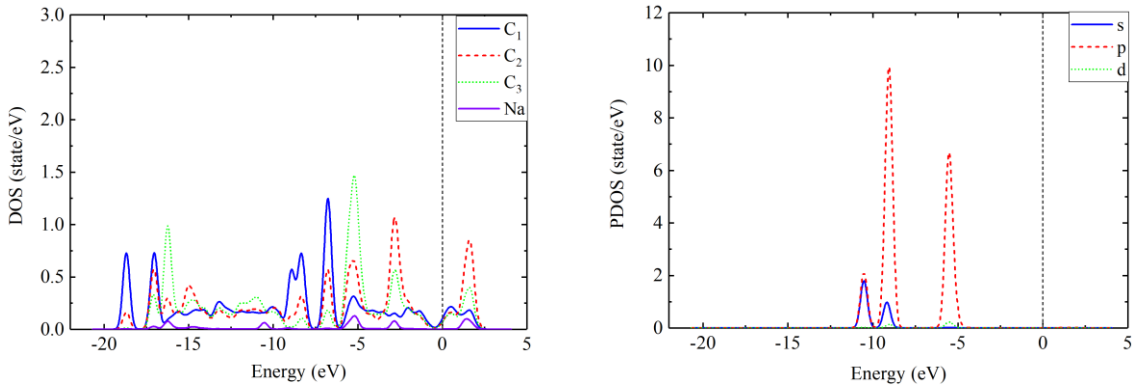
DOS (state/eV)
Energy (eV)
C1
C2
C3
Na
PDOS (state/eV)
Energy (eV)
s
p
d

(c)

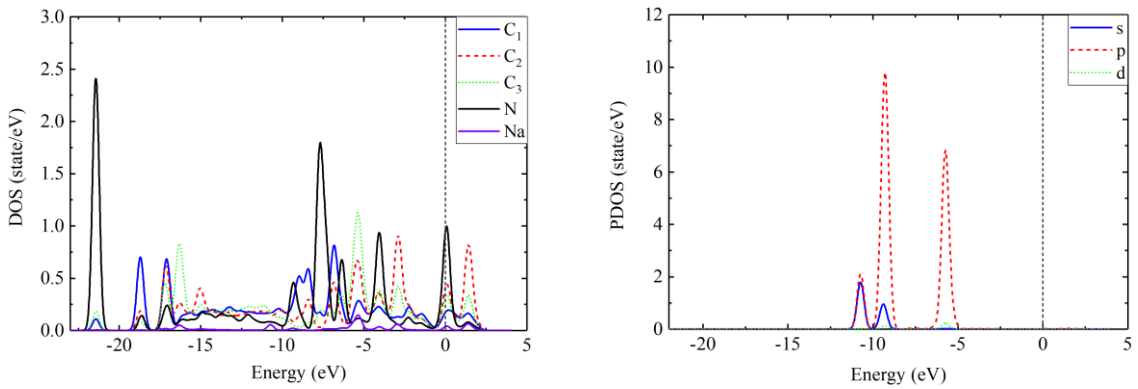

(d)

Fig. 9. PDOS images of the CO_2 adsorbed onto: **(a)** S1, **(b)** S2, **(c)** S3, and **(d)** S4 structures.

In the CO_2 molecule, the p-orbital contributes the most in states with two peaks in the energy range of 3.5eV and 7eV. As a preliminary conclusion, these peaks in structures decorated with Na atoms (S3 and S4) are in the lower energy range due to the Na atom's high electro-positivity. Unlike the smaller peak, having higher overlapping with the electrons of all three types of carbon atoms, the larger peak in the GDY structure has less overlap with the electrons of the carbon atom in its energy domain. The overlapping of the orbitals of the CO_2 molecule and the adsorbent, as observed in the PDOS of modified structures, could enhance the adsorbent performance in the adsorption of CO_2 gas molecules.

The distribution of p orbital electrons in the CO_2 molecule has changed in S2 compared to S1, and the height of the bigger (smaller) peak has decreased (increased), in addition to shifting the peaks to lower energy levels. In the S2 configuration, GDY's structural electrons overlap with the electrons of the N atom and the CO_2 molecule, increasing the released energy during the CO_2 adsorption process. Electrons of the s- and p-orbitals of the CO_2 molecule overlap with the electrons of the Na atom, as shown in **Figs. 9-(c) and 9-(d)**, enhancing the adsorption energy. The reduced overlap of electrons of structural carbon atoms and the CO_2 gas molecule

in the S4 is related to the altered electron distribution in the carbon atoms (due to the presence of the N atom). This is why the S3 structure adsorbs CO_2 molecules better than the S4 structure.

Fig. 10 depicts the differences in each electron-density distribution of structure to provide additional evidence for the CO_2 capturing results. The blue and red regions in **Fig. 10** show electron depletion and enhancement, respectively. The white lines between the blue and red regions indicate a slight change in electron density. As can be seen, the presence of Na at the H3 position creates an electron enhancement area in the adsorbent structure, resulting in a secondary electric field. As a result of their higher interaction with CO_2, S3 and S4 structures are better suited for trapping gas molecules.

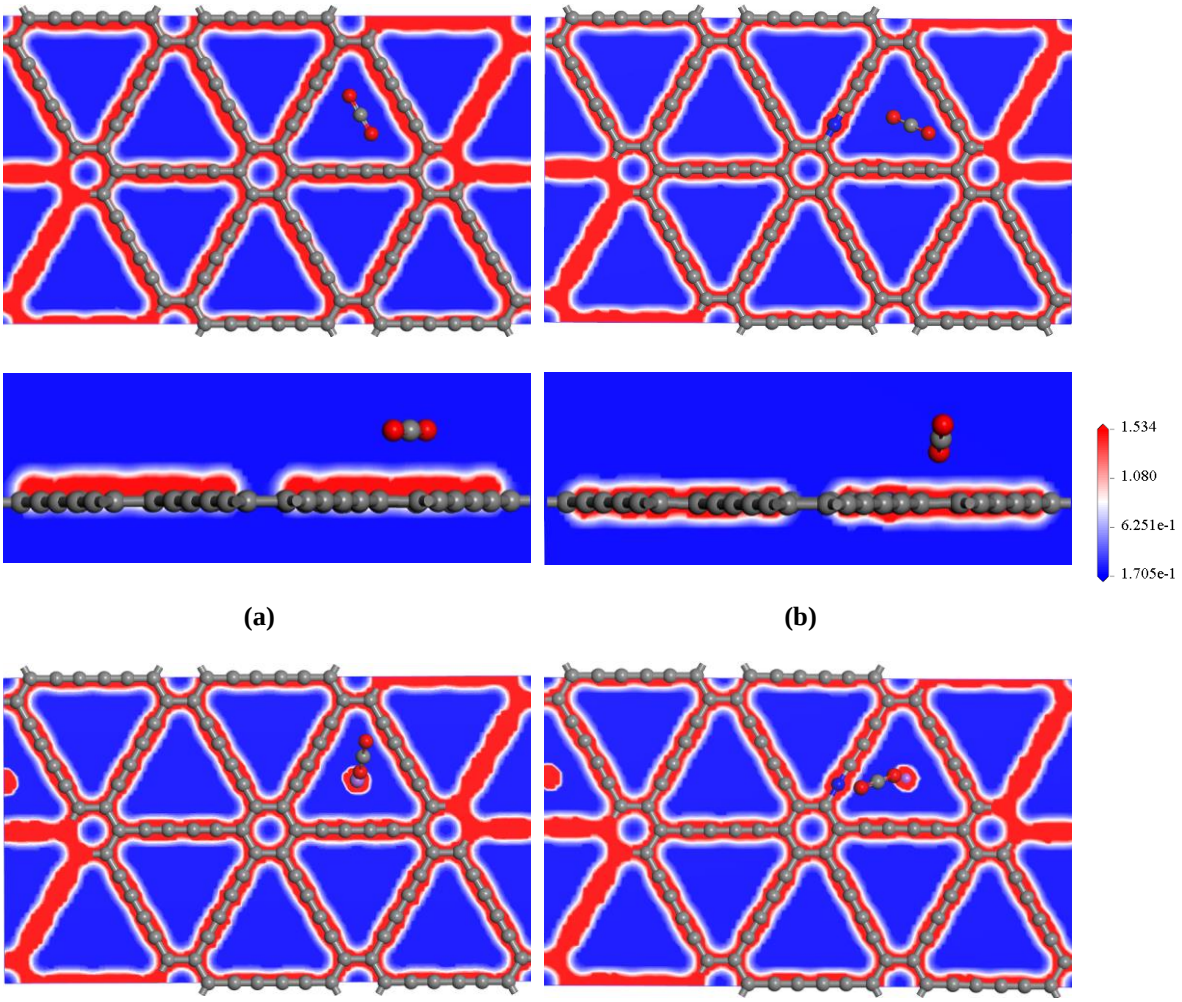

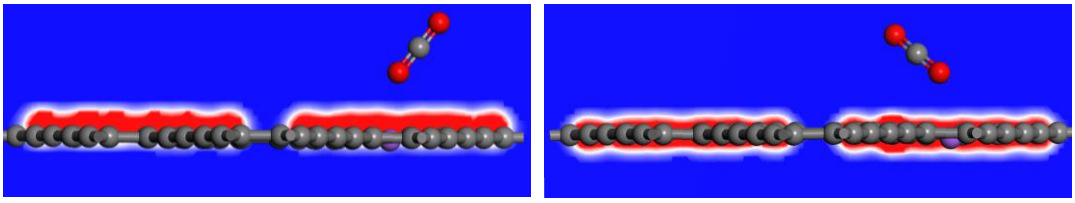

(c) **(d)**

Fig. 10. The difference electron density images of adsorbed CO_2 onto **(a)** S1, **(b)** S2, **(c)** S3, and **(d)** S4 structures.

3.3. Capture capacity of CO_2 molecules onto the pristine and modified GDY

After geometry optimization of the S1-S4 structures, all the possibilities for adsorption of the first CO_2 were investigated. Afterward, the most stable configuration was used for placing the second CO_2. Again, all the possible positions for the adsorption of the second CO_2 were considered, and this procedure was repeated for the adsorption of all the CO_2 molecules. The amount of CO_2 the absorbent captures is a crucial consideration for determining the best structure. CO_2 molecules were subsequently introduced to the structures to assess the performance of the adsorbents from the standpoint of CO_2 capture. The system (adsorbent+ nCO_2) was optimized at each stage, and the average adsorption energy (E_{ads}) and phase adsorption energy (E_s) were computed. The US Department of Energy has set the energy value Es=0.1eV as a criterion for determining the maximum amount of CO_2 adsorption capability. Thus, to estimate the maximum adsorption capacity of each structure, placing the CO_2 molecule on the structure continued until the E_s of the step became less than this threshold energy. The E_{ads} and E_s, C-O bond length, O-C-O angle, and hydrogen storage capacity (Wt %) for all four structures are listed in **Table 6**.

Table 6. E_{ads} and Es (eV), C-O bond length (L_{C-O}), O-C-O angle, and maximum CO_2 capture capacity (wt. %) in S1, S2, S3, and S4 structures.

Struc.	# CO_2	E_{ads}(eV)	E_s(eV)	L_{C-O}(Å)	∠O-C-O	Wt. %	Struc.	# CO_2	E_{ads}(eV)	E_s(eV)	L_{C-O}(Å)	∠O-C-O	Wt. %
S1	1	-0.232	-0.232	1.175 1.175	179.646		S3	1	-0.432	-0.432	1.179 1.167	179.283	
	2	-0.207	-0.183	1.175 1.175	179.631			2	-0.427	-0.421	1.180 1.166	179.586	
	3	-0.228	-0.269	1.175 1.175	179.253			3	-0.405	-0.361	1.180 1.169	178.763	
	4	-0.227	-0.224	1.176 1.174	179.193	44.87%		4	-0.378	-0.299	1.176 1.173	179.889	
	5	-0.199	-0.090	1.177 1.175	179.730			5	-0.384	-0.407	1.179 1.169	179.342	
S2	1	-0.271	-0.271	1.176 1.174	179.173			6	-0.363	-0.259	1.176 1.174	179.796	52.46%
	2	-0.344	-0.416	1.176 1.174	179.079			7	-0.325	-0.098	1.170 1.177	179.197	
	3	-0.304	-0.226	1.175 1.176	179.288		S4	1	-0.442	-0.442	1.167 1.181	179.214	
	4	-0.285	-0.227	1.176 1.175	179.134			2	-0.424	-0.406	1.169 1.179	178.855	
	5	-0.268	-0.199	1.176 1.175	179.753			3	-0.442	-0.367	1.176 1.173	179.653	
	6	-0.255	-0.191	1.176 1.175	179.678			4	-0.387	-0.223	1.177 1.169	179.870	
	7	-0.293	-0.230	1.176 1.174	179.784			5	-0.396	-0.432	1.176 1.173	179.565	
	8	-0.246	-0.209	1.176 1.174	179.741			6	-0.401	-0.424	1.167 1.180	178.628	
	9	-0.236	-0.158	1.176 1.174	179.665			7	-0.434	-0.238	1.167 1.180	178.628	
	10	-0.233	-0.206	1.175 1.175	179.553			8	-0.334	-0.230	1.177 1.173	179.648	59.34%
	11	-0.232	-0.220	1.176 1.174	179.371	68.92%		9	-0.307	-0.096	1.172 1.777	179.324	
	12	-0.221	-0.093	1.178 1.173	179.195								

As previously reported, the bond length and angle of the free CO_2 molecule are determined to be 1.175Å and 179.66°, respectively. However, as seen during CO_2 capture, the bond length and angle of each CO_2 molecule vary and vary around the values observed for free CO_2. The number of CO_2 molecules adsorbed in each of the structures S1, S2, S3, and S4 is 4, 11, 6, and 8, corresponding to about 44.87, 68.92, 59.34, and 58.16 Wt%, respectively. After the final

417 CO_2 molecule was placed in the structure and the system was optimized, the energy released
418 by S1, S2, S3, and S4 was -0.090, -0.093, -0.098, and -0.096eV, respectively; this indicates
419 that the adsorbents' maximum CO_2 capture capability has been reached.

420 As shown in **Table 6**, doping N atoms inside the structure increases the CO_2 capture capacity
421 of the system by up to 1.5 times that of pure GDY. Although adding the Na atom to both the
422 S1 and S2 structures improves the adsorption capacity compared to the S1, the S2 structure is
423 a more storage-efficient structure obtained simply by doping the N atom onto the GDY. As
424 seen in **Fig. 10**, adorning the Na atom in the structure results in the formation of an electron
425 depletion zone, which can generate a secondary electric field in addition to the primary electric
426 field of the structure. As a result of the influence of the field on the CO_2 molecules during the
427 capturing process, the number of molecules captured in the adsorption site increased. **Fig. 11**
428 depicts the final CO_2-saturated system for all four structures (S1, S2, S3, and S4), and the state
429 of the CO_2 molecules on either side of the adsorbents.

430

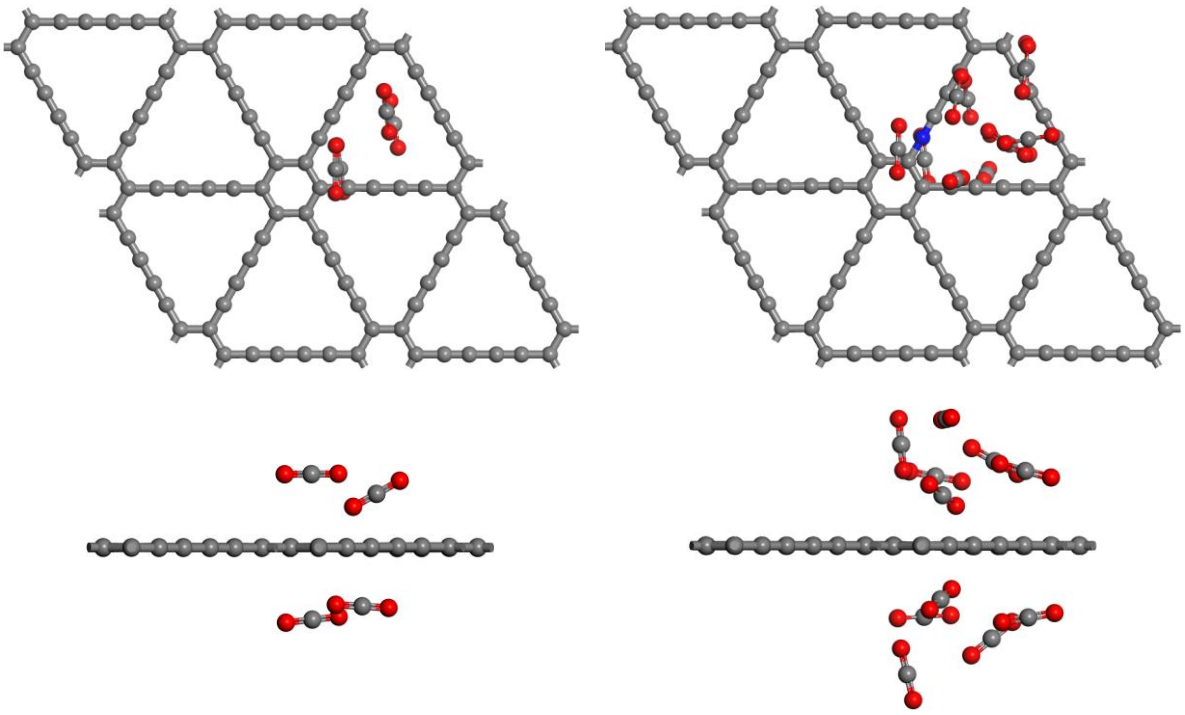

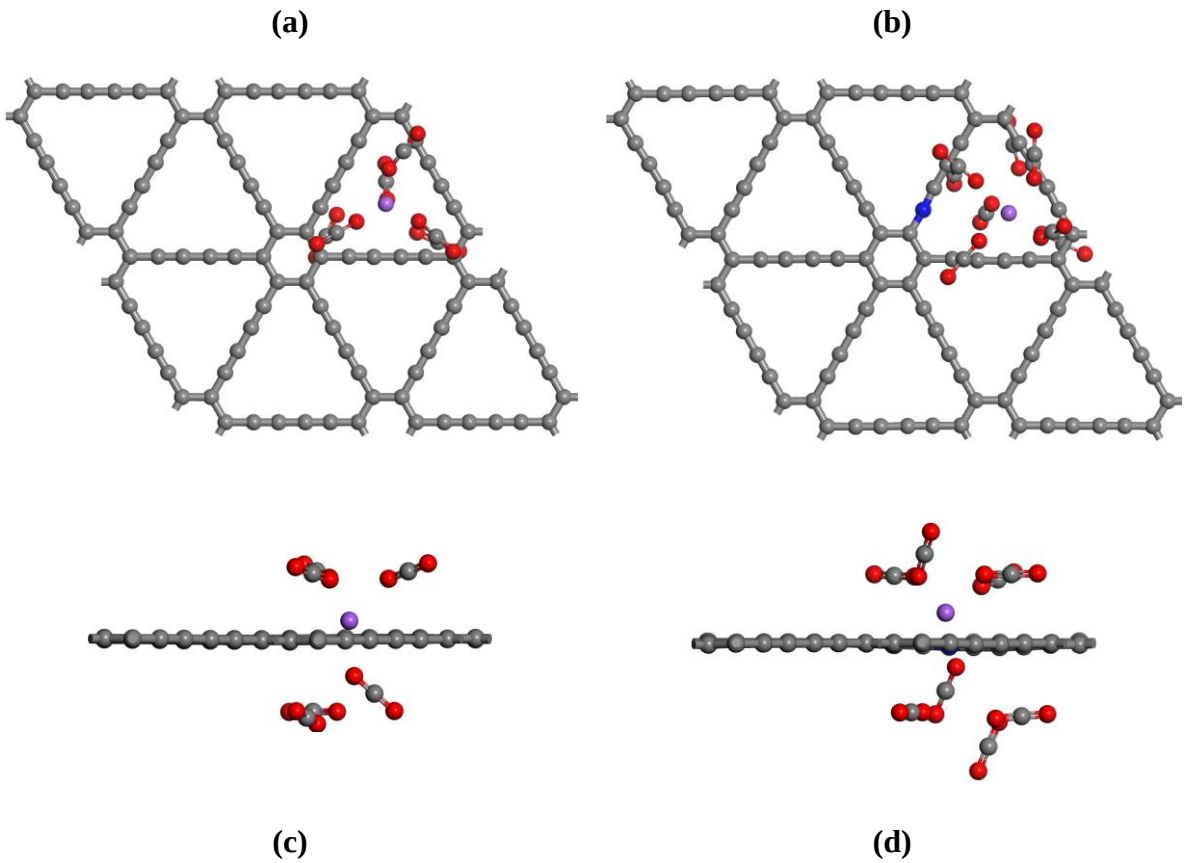

Fig. 11. Top and side views of the CO_2 storage of **(a)** S1-4CO_2, **(b)** S2-11CO_2, **(c)** S3-6CO_2, and (d) S4-8CO_2-systems.

Fig. 12 compares the CO_2 adsorption capacities of the structures with the adsorption energy expressed in terms of the number of adsorbed molecules. As can be observed, following the adsorption of the fourth CO_2 molecule with the adsorption energy of -0.227eV, the structure of S1 is saturated. The doped N atom in the S2 structure enhances the CO_2 adsorption capacity about threefold (11CO_2), with a final adsorption energy of -0.232eV. In the S3, the Na-decorating increases the amount of adsorbed CO_2 molecules up to 1.5 times, with a final adsorption energy of -0.363eV. However, the number of adsorbed molecules improved for the S4 structure by up to twofold, having a slightly lower final adsorption energy (-0.334eV).

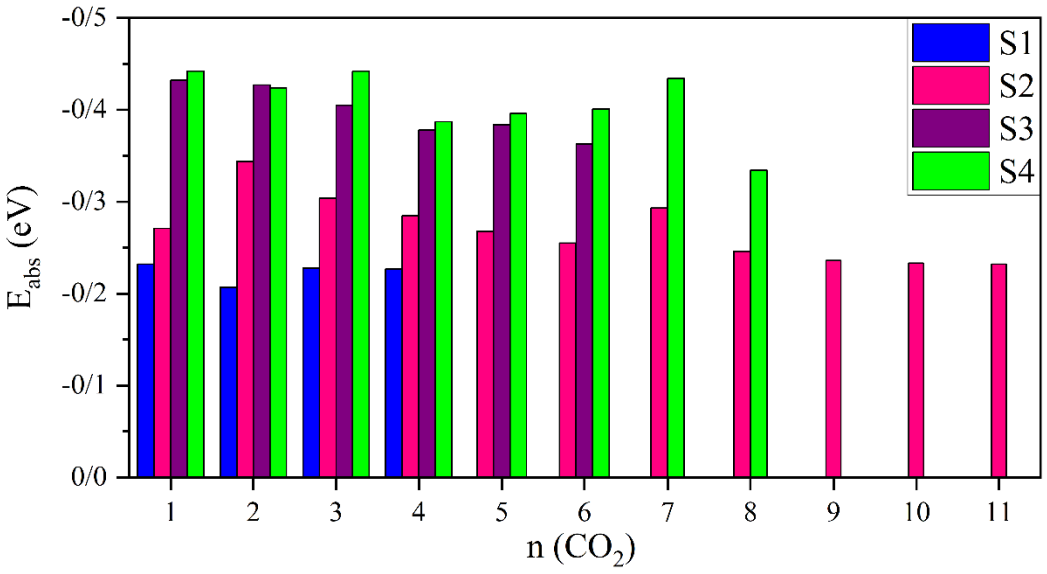

443 **Fig. 12.** Comparison of the mean adsorption energy of each step against the number of CO_2 molecules for S1,
444 S2, S3, and S4 structures.

445

446 **4. Conclusion**

447 The DFT-D2 approach was used to investigate the impacts of modifications such as N-doping,
448 Na-decoration and their combination on the structural and electronic properties of GDY as well
449 as the adsorption behavior of single CO_2. By substituting N for the C2 atom, the best N-doped
450 GDY is obtained (E_{coh} =-7.231eV), and by inserting a Na atom in the H3 site, the most stable
451 Na-decorated GDY is obtained (E_{ads} =-3.804eV). H3 was also shown to be the optimal site for
452 Na-decorating with E_{ads} =-0.432eV. The electronic properties of all structures were also
453 investigated, including TDOS and band structures and atomic charge. To explore single CO_2
454 capture, CO_2 molecules were initially positioned horizontally and vertically in the pristine and
455 best-modified GDY structure at H1, H2, H3, B, and M locations. The results indicated that for
456 S1, S2, and S3, H3 is the optimal site, whereas M is the optimal site for CO_2 adsorption on S4.
457 Also, the maximum value of adsorption energy was equal to about (40 $kJ.mol^{-1}$), which is

assumed that the adsorption of CO_2 on the nanosheets is physical and driven by Vander Waals forces [43].

Finally, each structure's maximal CO_2 capture capacity was determined by bringing CO_2 molecules close to the adsorbent and optimizing the resulting system. The results of this section indicate that S2 (N-doped GDY) has almost threefold the CO_2 capturing capability of S1 (pristine GDY); thus, it is a candidate for future CO_2 capture, storage, detection, and removal applications.

Acknowledgments

M. A.B. and Z. B. are grateful to the Research Council of the Lorestan University.

References

[1] Gurkan B, Goodrich BF, Mindrup EM, Ficke LE, Massel M, Seo S, et al. Molecular design of high capacity, low viscosity, chemically tunable ionic liquids for CO2 capture. J Phys Chem Lett 2010;1:3494–9.

[2] Venkataramanan NS, Suvitha A, Mizuseki H, Kawazoe Y. Functionalized Nanofullerenes for Hydrogen Storage: A Theoretical Perspective. ArXiv Prepr ArXiv11064524 2011.

[3] Li J, Hou M, Chen Y, Cen W, Chu Y, Yin S. Enhanced CO2 capture on graphene via N, S dual-doping. Appl Surf Sci 2017;399:420–5.

[4] Darvishnejad MH, Reisi-Vanani A. Synergetic effects of metals in graphyne 2D carbon structure for high promotion of CO2 capturing. Chem Eng J 2021;406:126749.

[5] Zou L, Zhu Y, Cen W, Jiang X, Chu W. N-doping in graphdiyne on embedding of metals and its effect in catalysis. Appl Surf Sci 2021;557:149815.

[6] Gu H, Zhong L, Shi G, Li J, Yu K, Li J, et al. Graphdiyne/Graphene Heterostructure: A Universal 2D Scaffold Anchoring Monodispersed Transition-Metal Phthalocyanines for Selective and Durable CO2 Electroreduction. J Am Chem Soc 2021.

[7] Luo G, Qian X, Liu H, Qin R, Zhou J, Li L, et al. Quasiparticle energies and excitonic effects of the two-dimensional carbon allotrope graphdiyne: Theory and experiment. Phys Rev B 2011;84:75439.

[8] Zhang S, Du H, He J, Huang C, Liu H, Cui G, et al. Nitrogen-doped graphdiyne applied for lithium-ion storage. ACS Appl Mater \& Interfaces 2016;8:8467–73.

[9] Sun C, Searles DJ. Lithium storage on graphdiyne predicted by DFT calculations. J Phys Chem C 2012;116:26222–6.

[10] Wang S, Yi L, Halpert JE, Lai X, Liu Y, Cao H, et al. A novel and highly efficient photocatalyst based on P25--graphdiyne nanocomposite. Small 2012;8:265–71.

[11] Liu T, Wang Q, Wang G, Bao X. Electrochemical CO 2 reduction on graphdiyne: a DFT study. Green Chem 2021;23:1212–9.

[12] Li G, Li Y, Liu H, Guo Y, Li Y, Zhu D. Architecture of graphdiyne nanoscale films. Chem Commun 2010;46:3256–8.

[13] Niaei AHF, Hussain T, Hankel M, Searles DJ. Sodium-intercalated bulk graphdiyne as an anode material for rechargeable batteries. J Power Sources 2017;343:354–63.

[14] Jiao Y, Du A, Hankel M, Zhu Z, Rudolph V, Smith SC. Graphdiyne: a versatile nanomaterial for electronics and hydrogen purification. Chem Commun 2011;47:11843–5.

[15] Ebadi M, Reisi-Vanani A. Methanol and carbon monoxide sensing and capturing by pristine and Ca-decorated graphdiyne: A DFT-D2 study. Phys E Low-Dimensional Syst Nanostructures 2021;125:114425.

[16] Wu Y, Chen X, Weng K, Jiang J, Ong W-J, Zhang P, et al. Highly Sensitive and Selective Gas Sensor Using Heteroatom Doping Graphdiyne: A DFT Study. Adv Electron Mater 2021:2001244.

[17] Li J, Zhong L, Tong L, Yu Y, Liu Q, Zhang S, et al. Atomic Pd on graphdiyne/graphene heterostructure as efficient catalyst for aromatic nitroreduction. Adv Funct Mater 2019;29:1905423.

[18] Kosar N, Shehzadi K, Ayub K, Mahmood T. Theoretical study on novel superalkali doped graphdiyne complexes: unique approach for the enhancement of electronic and nonlinear optical response. J Mol Graph Model 2020;97:107573.

[19] Xu P, Na N, Mohamadi A. Investigation the application of pristine graphdiyne (GDY) and boron-doped graphdiyne (BGDY) as an electronic sensor for detection of anticancer drug. Comput Theor Chem 2020;1190:112996.

[20] Ebadi M, Reisi-Vanani A, Houshmand F, Amani P. Calcium-decorated graphdiyne as a high hydrogen storage medium: evaluation of the structural and electronic properties. Int J Hydrogen Energy 2018;43:23346–56.

[21] Feng Z, Tang Y, Ma Y, Li Y, Dai Y, Ding H, et al. Theoretical investigation of CO2 electroreduction on N (B)-doped graphdiyne mononlayer supported single copper atom. Appl Surf Sci 2021;538:148145.

[22] Darvishnejad MH, Reisi-Vanani A. Multiple CO2 capture in pristine and Sr-decorated graphyne: A DFT-D3 and AIMD study. Comput Mater Sci 2020;176:109539.

[23] Yang C, Wang Y, Yu J, Cao S. Ultrathin 2D/2D Graphdiyne/Bi2WO6 Heterojunction for Gas-Phase CO2 Photoreduction. ACS Appl Energy Mater 2021;4:8734–8.

[24] Dang Y, Guo W, Zhao L, Zhu H. Porous carbon materials based on graphdiyne basis units by the incorporation of the functional groups and Li atoms for superior CO2 capture and sequestration. ACS Appl Mater \& Interfaces 2017;9:30002–13.

[25] Bie C, Cheng B, Ho W, Li Y, Macyk W, Ghasemi JB, et al. Graphdiyne-based photocatalysts for solar fuel production. Green Chem 2022;24:5739–54. https://doi.org/10.1039/d2gc01684b.

[26] Perdew JP, Burke K, Ernzerhof M. Generalized gradient approximation made simple. Phys Rev Lett 1996;77:3865.

[27] Delley B. Hardness conserving semilocal pseudopotentials. Phys Rev B 2002;66:155125.

[28] Delley B. From molecules to solids with the DMol 3 approach. J Chem Phys 2000;113:7756–64.

[29] Akbari F, Reisi-Vanani A, Darvishnejad MH. DFT study of the electronic and structural properties of single Al and N atoms and Al-N co-doped graphyne toward hydrogen storage. Appl Surf Sci 2019;488:600–10.

[30] Ehrlich S, Moellmann J, Reckien W, Bredow T, Grimme S. System-dependent dispersion coefficients for the DFT-D3 treatment of adsorption processes on ionic surfaces. ChemPhysChem 2011;12:3414–20.

[31] Grimme S, Antony J, Ehrlich S, Krieg H. A consistent and accurate ab initio parametrization of density functional dispersion correction (DFT-D) for the 94 elements H-Pu. J Chem Phys 2010;132:154104.

549 [32] Grimme S. Semiempirical GGA-type density functional constructed with a long-range
550 dispersion correction. J Comput Chem 2006;27:1787–99.

551 [33] Monkhorst HJ, Pack JD. Special points for Brillouin-zone integrations. Phys Rev B
552 1976;13:5188.

553 [34] Harrison RW, Lee WE. Processing and properties of ZrC, ZrN and ZrCN ceramics: a
554 review. Adv Appl Ceram 2016;115:294–307.

555 [35] Lombardi EB, Mainwood A, Osuch K, Reynhardt EC. Computational models of the
556 single substitutional nitrogen atom in diamond. J Phys Condens Matter 2003;15:3135–
557 49. https://doi.org/10.1088/0953-8984/15/19/314.

558 [36] Li C, Li J, Wu F, Li SS, Xia JB, Wang LW. High capacity hydrogen storage in Ca
559 decorated graphyne: A first-principles study. J Phys Chem C 2011;115:23221–5.
560 https://doi.org/10.1021/jp208423y.

561 [37] Hu L, Hu X, Wu X, Du C, Dai Y, Deng J. Density functional calculation of transition
562 metal adatom adsorption on graphene. Phys B Condens Matter 2010;405:3337–41.
563 https://doi.org/10.1016/j.physb.2010.05.001.

564 [38] He F. Basic Structure and Band Gap Engineering: Theoretical Study of GDYs.
565 GraphdiyneFundamentals Appl. Renew. Energy Electron., John Wiley & Sons, Ltd;
566 2022, p. 13–77. https://doi.org/https://doi.org/10.1002/9783527828470.ch2.

567 [39] Liu X, Wang Z, Tian Y, Zhao J. Graphdiyne-Supported Single Iron Atom: A
568 Promising Electrocatalyst for Carbon Dioxide Electroreduction into Methane and
569 Ethanol. J Phys Chem C 2020;124:3722–30. https://doi.org/10.1021/acs.jpcc.9b11649.

570 [40] S. sheng L. Semiconductor Physical Electronics. Semicond Phys Electron 2006.
571 https://doi.org/10.1007/0-387-37766-2.

572 [41] Guillory JK. Book Review of CRC Handbook of Chemistry and Physics. 2009.

573 [42] Enujekwu FM, Ezeh CI, George MW, Xu M, Do H, Zhang Y, et al. A comparative
574 study of mechanisms of the adsorption of CO 2 confined within graphene--MoS 2
575 nanosheets: a DFT trend study. Nanoscale Adv 2019;1:1442–51.

576 [43] Mahmood Aljamali N, Obaid Alfatlawi I. Physical and Chemical Adsorption and its
577 Applications. Int J Thermodyn Chem Kinet 2021;7. https://doi.org/10.37628/IJTCK.

578